

Vacancy-mediated suppression of phase separation in a model two-dimensional surface alloy by the difference of the atomic jump rates

Mikhail Khenner^{*1,2}

¹*Department of Mathematics, Western Kentucky University, Bowling Green, KY 42101, USA*

²*Applied Physics Institute, Western Kentucky University, Bowling Green, KY 42101, USA*

(Dated: April 20, 2022)

A vacancy-mediated collective diffusion model is used to compute a thermally-induced (spinodal) phase separation in a typical fcc bi-metallic surface alloy at low median concentration of vacancies, focusing on the effect of the ratio, $\Gamma = \Gamma_A/\Gamma_B$, of the jump rates to the vacant sites of the two types of atoms. The model is formulated for the diffusion of one atomic species and vacancies, employing the kinetic transport coefficients derived by Moleko *et al.* (Phil. Mag. A 59, 141 (1989)). It is demonstrated that for $A_{0.7}B_{0.3}$ alloy, $\Gamma \sim 50$ results in suppression of phase separation, whereas very small Γ values result in mild phase separation (i.e., the suppression is incomplete).

Keywords: surface alloys; vacancy-mediated diffusion; phase separation.

I. INTRODUCTION

Bi-metallic surface alloys are important materials for catalysis [1], since they can exhibit an improved catalytic activity through tailoring the concentration and/or the arrangement of two metallic components. Design of surface catalysts can benefit from surface phase-separated states for enhanced area-selective catalytic activity [2]. Moreover, certain metal/semi-metal surface alloys are topological insulators, where “the quantum confinement effect can suppress the bulk conduction channels and enhance the transport of the topological surface states” [3]. This property is valuable for design of future electronic and spintronic devices [4, 5]. If present, surface phase separation significantly affects surface electrical conductivity and therefore, it is bound to interfere with device performance.

For bimetallic surfaces, it is often difficult to determine, based on purely thermodynamic (energy-based) arguments, whether phase separation occurs [6–8], in part because a typical surface at a temperature significantly below its melting temperature is metastable, i.e. a non-equilibrium stationary structure may be kinetically stabilized by the presence of high energy barriers hindering the transition to an equilibrium state [9]. On the other hand, in metal surfaces, structural rearrangements typically occur through vacancy-mediated diffusion [8, 10–13]. Therefore, understanding kinetic factors influencing vacancy-mediated diffusive phase separation in binary surface alloys is important, but we are not aware of any experiment or model/computational study that addresses this issue.

The ratio of the jump rates to the vacant sites of the two types of atoms in a binary alloy, $\Gamma = \Gamma_A/\Gamma_B$, is the most important kinetic factor governing vacancy-mediated diffusion. In this communication, we fill the above-stated gap in knowledge by developing a “collective”, or “chemical” (i.e., a continuum) vacancy-mediated diffusion model and the corresponding computation, aiming to answer a single question: what is the effect of Γ on phase separation in a bi-metallic surface alloy ?

The physical assumptions that underlie our model are customary [14]: (i) the jump rates are constant, i.e. they do not depend on the occupation of the sites surrounding the vacant sites; (ii) the interactions between nearest neighbors atoms are pairwise, and (iii) the vacancies are conserved, which means that an atom from a surface monolayer cannot hop on top of a monolayer, thus creating a vacant site inside the monolayer, or an adatom executing surface diffusion cannot jump into a vacant site inside the monolayer. The consequence of this is that A and B atoms are conserved in the monolayer. Validity of the above assumptions has been confirmed by DFT calculations based on transition state theory [15].

II. THE MODEL

We consider a thin film of a uniform composition A, whereby the impurity B atoms are mixed into the topmost surface layer, thus creating a two-dimensional binary surface alloy. Vacancy-mediated diffusion of A and B is assumed to take place in the atomically thin surface layer.

* Corresponding author. E-mail: mikhail.khenner@wku.edu.

Since the model equations are somewhat cumbersome, we will state them immediately in the dimensionless form. Let $X_i(x, y, t)$ be the concentration, or the composition fraction, of the i -th species, defined as the number of atoms per unit area. Since each lattice site is occupied by an atom or a vacancy, the lattice site fraction is related to a concentration by $X_i = \nu C_i$, where ν is the lattice site density, having the same units as X_i , and $C_i(x, y, t)$ is the dimensionless concentration. In a perfect lattice, the number of lattice sites is conserved: $X_A + X_B + X_V = \nu$. Dividing this relation by ν gives the constraint on the dimensionless concentrations:

$$C_A(x, y, t) + C_B(x, y, t) + C_V(x, y, t) = 1. \quad (1)$$

Next, we choose the lattice spacing a as the length scale and $\bar{t} = kT\nu/(\gamma_B\lambda\Gamma_B)$ as the time scale. Here kT is Boltzmann's factor, γ_B (γ_A) the surface energy of atomically thin surface layer that is composed of B (A) atoms, λ the dimensionless geometric factor for fcc lattice, and Γ_B the surface jump rate of B atoms, i.e. the jump rate of B-V exchanges. The following dimensionless parameters are introduced: $G = \gamma_A/\gamma_B$, the ratio of the surface energies of the atomic components; $N = kT\nu/\gamma_B$: the alloy entropy; $\xi = \delta/a\gamma_B$: the Cahn-Hilliard gradient energy coefficient (where δ is the dimensional gradient energy coefficient); $\Gamma = \Gamma_A/\Gamma_B$: the ratio of the surface jump rates; $H_{i,j} = \epsilon_{i,j}/\gamma_B$, $i, j = A, B$: the ratio of the bond strength between atoms of the same or a different kind to the B-surface energy; and $Q > -1$: the quench parameter, defined by $T = T_c/(1 + Q)$, where T_c is the critical (spinodal) temperature. Positive Q values correspond to $T < T_c$, which is the interval of the temperatures where phase separation is expected.

Our approach is based on the general continuum framework for vacancy-mediated diffusion in binary alloys, as described by Allnatt & Lidiard [16]. Note that although there are three concentration variables C_A , C_B and C_V , due to the constraint (1), only two of them are independent. Therefore in the collective diffusion framework only the transport of one atomic species (B in our model) and vacancies is computed; the concentration field of the second atomic species (A in our model) is determined from Eq. (1).

The diffusion equations for C_B and C_V will follow from mass conservation:

$$\frac{\partial C_B}{\partial t} = -\nabla \cdot \mathbf{J}_B, \quad \frac{\partial C_V}{\partial t} = -\nabla \cdot \mathbf{J}_V, \quad (2)$$

where \mathbf{J}_B , \mathbf{J}_V are the diffusion fluxes, and $\nabla = (\partial_x, \partial_y)$.

Let L_{AA} , L_{AB} , L_{BA} and L_{BB} be the kinetic transport coefficients of the alloy components, μ_A , μ_B and μ_V the chemical potentials of the alloy components and vacancies. According to Allnatt & Lidiard [16] (p. 166, 174, 175)

$$\mathbf{j}_B = -[L_{BV}\nabla(\mu_V - \mu_A) + L_{BB}\nabla(\mu_B - \mu_A)], \quad (3)$$

$$\mathbf{j}_V = -[L_{VV}\nabla(\mu_V - \mu_A) + L_{VB}\nabla(\mu_B - \mu_A)], \quad (4)$$

where

$$L_{BV} = -(L_{BA} + L_{BB}), \quad L_{VB} = -(L_{AB} + L_{BB}), \quad L_{VV} = L_{AA} + L_{AB} + L_{BA} + L_{BB} \quad (5)$$

are the effective kinetic transport coefficients after the diffusion of the A species is eliminated.

The kinetic transport coefficients read:

$$L_{AA} = \Gamma C_A \left(1 - \frac{2\Gamma C_B}{\psi}\right), \quad L_{AB} = \frac{2}{\psi} \Gamma C_A C_B, \quad L_{BA} = L_{AB}, \quad L_{BB} = C_B \left(1 - \frac{2C_A}{\psi}\right), \quad (6)$$

where ψ is given by

$$\psi = \frac{1}{2} (M_0 + 2) (\Gamma C_A + C_B) - \Gamma - 1 + 2(C_A + \Gamma C_B) + \sqrt{\left[\frac{1}{2} (M_0 + 2) (\Gamma C_A + C_B) - \Gamma - 1\right]^2 + 2M_0\Gamma}. \quad (7)$$

In Eq. (7), $M_0 = 2f_0/(1 - f_0)$, where f_0 is the tracer correlation factor for fcc lattice. Eq. (6) stipulates that $L_{AA} \gg L_{BB}$ at $\Gamma \gg 1$, or $\Gamma_A \gg \Gamma_B$ (thus in this case A is the fast diffusing species); conversely, at $\Gamma \ll 1$, B is the fast diffusing species. At $\Gamma = 1$ (the ‘‘neutral’’ value) and $C_A = C_B = 0.5$, $L_{AA} = L_{BB}$. Eqs. (6) and (7) are the dimensionless versions of the kinetic transport coefficients derived by Moleko et al. [17], who extended earlier results by Manning [18]. Allnatt and Lidiard [16] note that ‘‘... although (the coefficients) were derived ... with a specific model (the ‘‘random alloy model’’) in mind the derivation given here is not obviously limited to that model. Furthermore, the argument is in no way limited to small vacancy fractions’’ Additionally, as noted in Ref. [19], computations by Murch and co-workers [20, 21] also point to validity of these relations for ordered alloys. (Further discussion of the relations (6) and (7) can be found in Ref. [22].)

The chemical potentials in Eq. (4) follow from alloy thermodynamics [23, 24]:

$$\mu_A = C_B \left(\frac{\partial \gamma}{\partial C_A} - \frac{\partial \gamma}{\partial C_B} \right) - \xi \nabla^2 C_A - (1 - Q^{-1} C_V) C_A, \quad (8)$$

$$\mu_B = -C_A \left(\frac{\partial \gamma}{\partial C_A} - \frac{\partial \gamma}{\partial C_B} \right) - \xi \nabla^2 C_B + (1 - Q^{-1} C_V) C_B, \quad (9)$$

$$\mu_V = Q (C_A^2 + C_B^2) - \frac{\partial \gamma}{\partial C_V} = Q (C_A^2 + C_B^2) + N \ln \frac{1 - C_V}{C_V}, \quad (10)$$

where the free energy

$$\gamma = G C_A + C_B + \frac{1}{2} (H_{AA} C_A^2 + H_{BB} C_B^2 + 2H_{AB} C_A C_B) + N [C_A \ln C_A + C_B \ln C_B + C_V \ln C_V + (1 - C_V) \ln (1 - C_V)]. \quad (11)$$

In Eq. (11) the first two terms constitute the weighted surface energy of the bi-component monolayer [6], whereas the terms in the parenthesis and bracket are the enthalpic [14] and entropic [24] contributions, respectively.

After C_A is eliminated from Eqs. (2)-(10) using Eq. (1), the mathematical model is finalized. C_A is determined as, $C_A = 1 - C_B - C_V$ after C_B and C_V were computed using Eqs. (2).

Although the model may be applied to a rather general binary surface alloy, the material parameters that we use in Sections IIB and III (see Table I) are closely matching fcc AgPt(111) surface alloy, where Ag is the deposited impurity species (B atoms in the model). Ref. [25] describes this surface alloy as “... a solid solution with a positive enthalpy of mixing, which leads to phase separation”. These authors found that deposition of Ag on Pt(111) and short annealing at a temperature slightly above 620K results in a compact Ag clusters of the average size 10Å (about three lattice spacings across) embedded in the topmost Pt layer. Such partial de-mixing within the surface layer is consistent with the phase diagram for a bulk AgPt alloy, which features a wide miscibility gap up to $T \sim 1400\text{K}$ [26]. The average 10Å size of two-dimensional Ag clusters is attributed to the balance of a lattice mismatch strain and the line (boundary) tension in the late stages of phase separation of the intermixed surface layer (the lattice mismatch of Ag and Pt is a moderate 4% value). In the initial and intermediate stages of phase separation the effect of strain cannot be discerned in the experiment, thus this effect is presumably minor. For that reason, and since the model’s continuum nature allows to compute only the initial and intermediate stages of phase separation (see Sec. III; this is sufficient to quantify the Γ -effect), we did not incorporate the strain into our model.

Physical parameter	Typical value
a	2.89×10^{-8} cm [25]
$\nu = a^{-2}$	9.18×10^{14} cm ⁻²
λ	1/6 [18]
f_0	0.7815 [18]
T	400 K [12]
γ_A	2.3×10^3 erg/cm ² [27]
γ_B	1.17×10^3 erg/cm ² [27]
$\epsilon_{AB} = 0.1\gamma_B$	117 erg/cm ²
$\epsilon_{AA}, \epsilon_{BB} = -0.1\gamma_B$	-117 erg/cm ²
δ	1.2×10^{-5} erg/cm [28]

TABLE I: Physical parameters.

A. Notes on implementation

The model as described above is still too complex for analysis and computation, due to the fact that the kinetic transport coefficients (and also the effective transport coefficients) are the highly nonlinear and cumbersome functions of the space-time dependent concentrations C_B and C_V . Therefore, we approximate the kinetic transport coefficients

by evaluating ψ (Eq. (7)) at $C_B = C_{B0}$, $C_V = C_{V0}$, where C_{B0} and C_{V0} are the median concentrations in the as-prepared surface alloy, that is, the initial values for the simulation. This approximation has a very mild effect on the kinetic transport coefficients in the entire unit interval of the C_B and C_V values [29] and moreover, in order to verify that results are not affected, a few simulations were done where the computation is periodically suspended, ψ is re-computed using the instantaneous median values of C_B and C_V , and the computation is resumed.

Notice that the term $N \ln \frac{1-C_V}{C_V}$ in Eq. (10) diverges at $C_V = 0, 1$. A similar term, $N \ln \frac{1-C_B}{C_B}$, emerges in Eqs. (8) and (9) when in $\partial\gamma/\partial C_A$, $\ln(1 - C_B - C_V)$ is approximated as $\ln(1 - C_B)$. This is valid as long as C_V is small, the requirement that holds very well in the computation (see Sec. III; this is the only assumption of C_V being small in the entire model formulation.) However, regularization of these logarithmic potentials is not needed, since the diffusion fluxes, Eqs. (3) and (4), are proportional to the gradients of the potentials. The gradients also are divergent at 0 and 1. Thus to facilitate computation, the divergent gradients are tapered by regularizing them as follows:

$$\nabla \ln \frac{1 - C_i}{C_i} = \frac{\nabla C_i}{C_i(C_i - 1)} \approx \frac{\nabla C_i}{(C_i + \beta)(C_i - 1 - \beta)}, \quad i = B, V \quad (12)$$

where $0 < \beta \ll 1$. The chosen value for the computation is $\beta = 0.01$.

Note that for the example system, e.g. Ag/Pt(111) surface alloy, the assumption of small C_V can be validated by computing the equilibrium vacancy concentration using the formula $n_v^{eq} = n \exp(-q_v/kT)$, where n_v^{eq} is the number of vacancies, n the number of surface sites, and q_v a vacancy formation energy. For Pt(111) surface $q_v = 0.62$ eV [30], for Ag(111) surface $q_v = 0.67$ eV [31]. Thus for AgPt(111) surface one can assume the average value $q_v = 0.645$ eV. Using this value, for the range of temperatures 300K-700K one obtains $1.46 \times 10^{-11} \leq n_v^{eq} \leq 2.271 \times 10^{-5}$ at $n = 1$, which means that only one surface atom out of 6.85×10^{10} (at $n_v^{eq} = 1.46 \times 10^{-11}$), or out of 4.4×10^4 (at $n_v^{eq} = 2.271 \times 10^{-5}$) is missing. Similar estimates of n_v^{eq} were obtained by the embedded atom model [10].

The computations in Sec. III use larger mean concentration $C_{V0} = 0.01$, since at significantly smaller values a computation based on a continuum model breaks down due to divergence of $\nabla C_V/C_V(C_V - 1)$ at $C_V \rightarrow 0$, which even the mathematical regularization described above does not reliably eliminate. It follows from the linear stability analysis in the next section and from computations that the Γ -effect is not sensitive to the magnitude of C_{V0} . Essentially, only the computation time is affected when C_{V0} is varied. Moreover, according to Ref. [14] the statistical properties of vacancy-mediated diffusion (such as the phase boundary for the order-disorder transition and tracer diffusion coefficients) in the limit $C_V \rightarrow 0$ are accurately reproduced if the vacancy concentration is on the order of a few percents. That paper adopts $C_{V0} = 0.04$ for kinetic Monte-Carlo computations.

Global conservation of C_B and C_V was checked during computation. The largest loss that occurred is 0.4%.

B. Linear stability analysis

From the linearized model equations in Sec. II, one obtains a quadratic equation for the growth rate $\omega(k_x, k_y)$ of the infinitesimal perturbations of a constant base state $C_B = C_{B0}$, $C_V = C_{V0}$. Here k_x , k_y are the perturbation wavenumbers. When both roots of this quadratic are negative for all k_x , k_y , the phase separation of the alloy does not occur. In this case all small perturbations of the initial condition $C_B = C_{B0}$, $C_V = C_{V0}$ decay. Phase separation emerges due to growth of the perturbations when one or both roots are positive in a certain domain of the perturbation wavenumbers. The largest positive root ω_l determines the domain of the unstable wavenumbers and the most dangerous wavenumber pair that corresponds to the maximum of the perturbation growth rate.[33] As shown in Fig. 1 the instability has a long-wavelength character and the $\omega_l(k_x, k_y)$ surface is symmetric over $k_x - k_y$ plane. For the computations in Sec. III the size of the square computational domain is always chosen equal to $5\lambda_{max}$, where $\lambda_{max} = 2\pi/k_x^{max} = 2\pi/k_y^{max}$ and $k_x^{max} = k_y^{max}$ is the pair of the most dangerous wavenumbers.

It can be noticed in Fig. 1(b) that ω_l^{max} is more sensitive to increasing Γ values, than to decreasing them. λ_{max} is not very sensitive to changing Γ , it slightly increases when Γ either decreases or increases from unity ($\lambda_{max} = 8.58, 7.74, 8.28$ at $\Gamma = 0.1, 1, 2$, respectively).

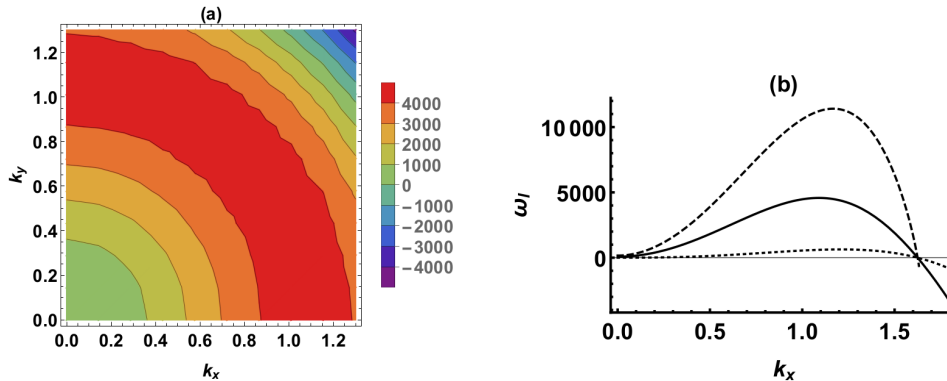


FIG. 1: (a) The contour plot of the perturbation growth rate, $\omega_l(k_x, k_y)$, at $Q = 0.005$ and $\Gamma = 1$. (b) The cross-section plots, $\omega_l(k_x, 1)$ at $Q = 0.005$ and $\Gamma = 1$ (solid line), $\Gamma = 2$ (dashed line), $\Gamma = 0.1$ (dotted line).

III. COMPUTATIONAL RESULTS

Computations of Eqs. (2) are performed on the square, bi-periodic domain of the size $5\lambda_{max}$. The initial condition is chosen as the constant concentration field of B atoms and a square vacancy island on the background of a very low constant concentration field of vacancies, that is, $C_B(x, y, 0) = C_{B0} = 0.3$, $C_V(x, y, 0) = C_{V0} + \eta(x, y) = 0.01 + \eta(x, y)$, where $\eta(x, y)$ is the "square box" function of the height 0.005 with a local support at the center of the computational domain. See Fig. 2. Such initial condition may be engineered by a low-energy focused ion beam irradiation of a surface, or by using other local tools to remove atoms from a surface, such as a tip of an atomic force microscope or a scanning tunneling microscope [32]. When the size of the computational domain changes due to λ_{max} change in response to a changes in the values of the material parameters Γ and Q , the local support of the island is changed to preserve the relative size of the island. (Notice that the initial data above and the fact that $C_{A0} = 1 - C_B(x, y, 0) - C_V(x, y, 0)$ yield $0.685 \leq C_{A0} \leq 0.69$.)

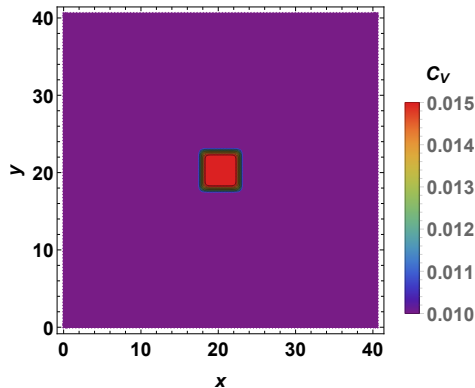


FIG. 2: The vacancy concentration field at $t = 0$.

As the computation of the phase separation progresses, the concentration of vacancies may vanish in some sub-region. In our setup, this typically happens fast due to the initial vacancy concentration being small already. Such event corresponds to the local composition attaining a value pair C_{Blocal} and $C_{Alocal} = 1 - C_{Blocal}$. In this case the computation is aborted and declared completed, and the concentrations are deemed final.

Figure 3 shows the final concentration fields at $\Gamma = 1, 10$ and 50 just above the threshold of a phase separation instability ($Q = 0.005$). A close inspection reveals very different outcomes. A common feature is the formation of a vacancy denuded zone around the vacancy island, which had shrunken in size. At $\Gamma = 1$ this zone extends to the entire exterior of the island (Fig. 3(b)). Vacancies flow to the center of the island from the exterior; at $\Gamma = 1$ the vacancy concentration increases ten-fold at the island center. This is accompanied by the C_B increase at the island center from 0.3 to 0.4 (33% increase) and a similar sized C_A decrease from 0.685 to 0.45 (Fig. 3(a,c)). In contrast, on the periphery of the vacancy island C_B decreases and C_A increases. The phase separation is evident in Figures 3(a,c).

As Γ increases, the vacancy denuded zone forms a ring around the island (Fig. 3(e)), and the ring breaks into several sections with the further Γ increase (Fig. 3(h)). Simultaneously, the vacancy concentration at the island center increases more moderately (but still by the factor of four in Fig. 3(h)), and C_B deviates less from the initial value 0.3 as Γ increases. In Fig. 3(g) it equals to the initial value everywhere. C_A still experiences a small decrease from 0.685 to 0.66 at the island center (3.6% difference, Fig. 3(i)) and the increase to 0.7 in the ring sections where the vacancy concentration dropped to zero. Overall, at $\Gamma = 50$ the phase separation is effectively terminated.

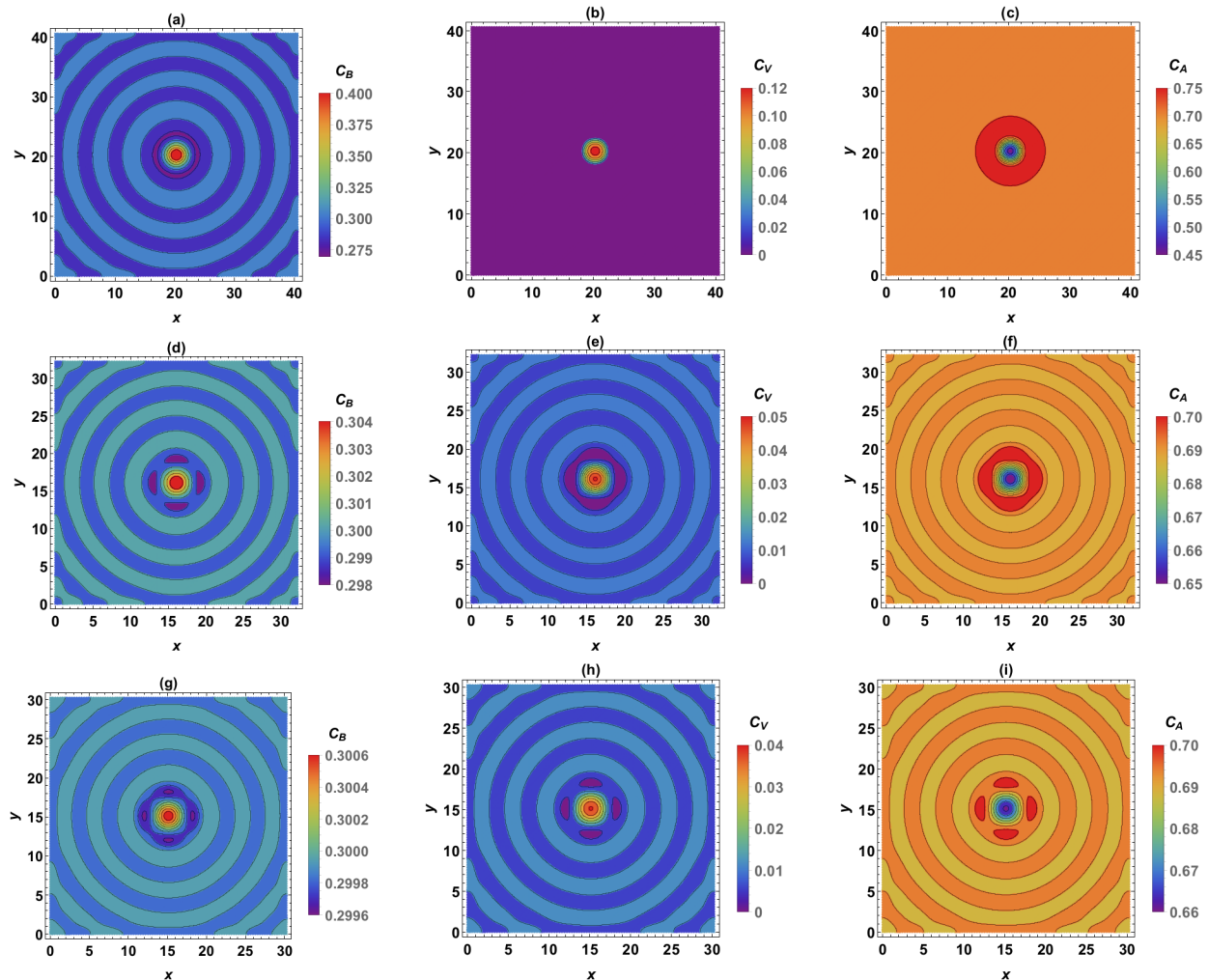


FIG. 3: (a), (b), (c): Final C_B , C_V and C_A at $\Gamma = 1$. (d), (e), (f): Final C_B , C_V and C_A at $\Gamma = 10$. (g), (h), (i): Final C_B , C_V and C_A at $\Gamma = 50$. $Q = 0.005$.

Decreasing Γ does not have the same effect as increasing it. In Fig. 4(a,c) it is seen that at $\Gamma = 0.002$ the phase separation is comparable to Fig. 3(d,f). However, in the latter figure Γ was increased only ten-fold from the neutral value $\Gamma = 1$, whereas in the former figure Γ was decreased from that value by the factor of five hundred. Also there appear the small-scale features in the C_B and C_A concentration fields inside the boundary of the vacancy island. The vacancy island itself has broken into four smaller islands, where C_V is four times larger than the initial value.

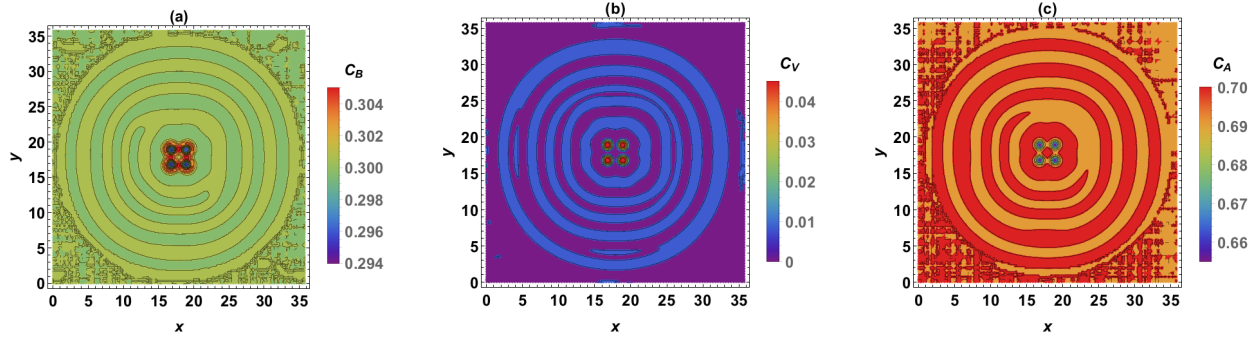


FIG. 4: (a), (b), (c): Final C_B , C_V and C_A at $\Gamma = 0.002$. $Q = 0.005$.

Finally, one can observe in Fig. 5 that moving away from the instability threshold via increasing Q , while keeping Γ equal to the neutral value, has the effect similar to the one in Fig. 4. Predictably, the phase separation diminishes, but it does not cease completely.

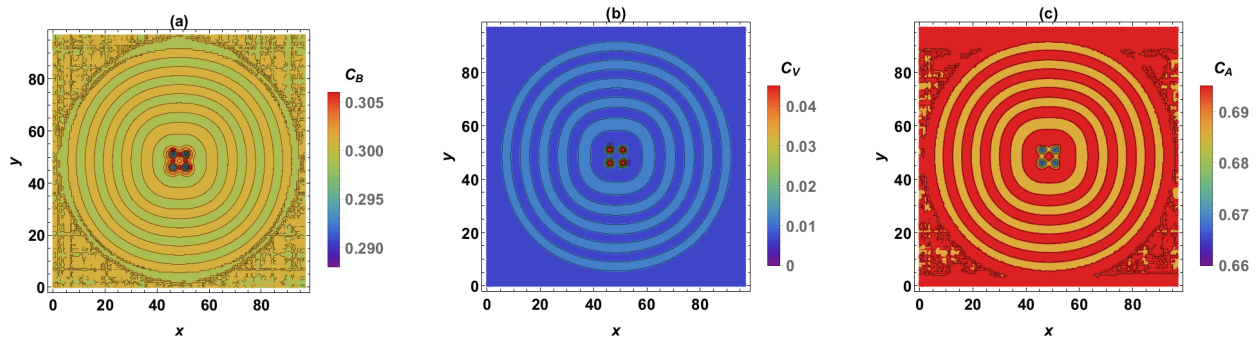


FIG. 5: (a), (b), (c): Final C_B , C_V and C_A at $\Gamma = 1$. $Q = 0.05$.

To summarize, the computations based on our chemical diffusion model of a typical 2D fcc surface alloy with a low vacancies concentration demonstrate that a phase separation instability is suppressed when the ratio of the jump rates Γ_A/Γ_B is around fifty, provided that A is the more abundant atomic species. The phase separation is present, but it is very mild (on the order of 1-2%) when A is the slow or very slow diffusing atomic species.

-
- [1] I. Song, “Surface alloys in nanochemistry: catalysis and synthesis”, *New J. Chem.* **44**, 18525 (2020).
 - [2] X. Fu, J. Liu, S. Kanchanakungwankul, X. Hu, Q. Yue, D. G. Truhlar, J.T. Hupp, and Y. Kang, “Two-Dimensional Pd Rafts Confined in Copper Nanosheets for Selective Semihydrogenation of Acetylene”, *Nano Lett.* **21**, 5620–5626 (2021).
 - [3] S. Xing, L. Lei, H. Dong, J. Guo, F. Cao, S. Gu, Y. Geng, S. Mi, H. Wu, F. Pang, W. Ji, R. Xu, and Z. Cheng, “Epitaxial fabrication of topological Bi-Sb alloy films by surface alloying of Sb nanofilms”, *Surf. Sci.* **714**, 121921 (2021).
 - [4] Y.-H. Su, W. Shi, C. Felser, Y. Sun, “Topological Weyl semimetals in $\text{Bi}_{1-x}\text{Sb}_x$ alloys”, *Phys. Rev. B* **97**, 155431 (2018).
 - [5] K.N.H. Duy, Y. Ueda, H.P. Nam, “A conductive topological insulator with large spin Hall effect for ultralow power spin-orbit torque switchings”, *Nat. Mater.* **17**, 808-813 (2018).
 - [6] A.V. Ruban, H.L. Skriver, and J.K. Norskov, “Local equilibrium properties of metallic surface alloys”, in: *The Chemical Physics of Solid Surfaces*, Ed.: D.P. Woodruff, vol. 10, Elsevier (2002).
 - [7] A. Christensen, A.V. Ruban, P. Stoltze, K.W. Jacobsen, H.L. Skriver, J.K. Norskov, and F. Besenbacher, “Phase diagrams for surface alloys”, *Phys. Rev. B* **56**, 5822 (1997).
 - [8] H. Hoster, “Properties of Surface Alloys”, in: *Surface and Interface Science*, vol.3: Properties of Composite Surfaces: Alloys, Compounds, Semiconductors, Ed.: K. Wandelt, Wiley-VCH Verlag GmbH & Co (2014).
 - [9] E. Bussmann, I. Ermanoski, P. J. Feibelman, N. C. Bartelt, and G. L. Kellogg, “Buried Pd slows self-diffusion on Cu(001)”, *Phys. Rev. B* **84**, 245440 (2011).
 - [10] R. van Gastel, E. Somfai, S.B. van Albada, W. van Saarloos, and J.W.M. Frenken, “Nothing moves a surface: Vacancy-mediated surface diffusion”, *Phys. Rev. Lett.* **86**, 1562 (2001).
 - [11] M.L. Grant, B.S. Swartzentruber, N.C. Bartelt, and J.B. Hannon, “Diffusion kinetics in the Pd/Cu(001) surface alloy”, *Phys. Rev. Lett.* **86**, 4588 (2001).

- [12] M.L. Anderson, M.J. D'Amato, P.J. Feibelman, and B.S. Swartzentruber, "Vacancy-mediated and exchange diffusion in a Pb/Cu(111) surface alloy: Concurrent diffusion on two length scales", *Phys. Rev. Lett.* **90**, 126102 (2003).
- [13] R. van Gastel, E. Somfai, W. van Saarloos, and J.W.M. Frenken, "A giant atomic slide-puzzle", *Nature* **408**, 665 (2000).
- [14] A. De Virgiliis and K. Binder, "Interplay of order-disorder phenomena and diffusion in rigid binary alloys in the presence of vacancies: Monte Carlo simulations", *Phys. Rev. B* **73**, 134205 (2006).
- [15] D. Mahlberg and A. Grob, "Vacancy assisted diffusion on single-atom surface alloy", *ChemPhysChem* **22**, 29 (2021).
- [16] A.R. Allnatt and A.B. Lidiard, "Atomic transport in solids", *Cambridge University Press*, Cambridge, UK (1993).
- [17] L.K. Moleko, A.R. Allnatt, and E.L. Allnatt, "A self-consistent theory of matter transport in a random lattice gas and some simulation results", *Phil. Mag. A* **59**, 141 (1989).
- [18] J.R. Manning, "Correlation factors for diffusion in nondilute alloys", *Phys. Rev. B* **4**, 1111 (1971).
- [19] H. Mehrer, *Diffusion in solids*. Springer (2007).
- [20] I.V. Belova and G.E. Murch, "Test of the validity of the Darken/Manning relation for diffusion in ordered alloys taking the L12 structure", *Philos. Mag. A* **78**, 1085 (1998).
- [21] I.V. Belova and G.E. Murch, "The Manning relations for atomic diffusion in a binary ordered alloy", *Philos. Mag. A* **75**, 1715 (1997).
- [22] A. Van der Ven, H.-C. Yu, G. Ceder, and K. Thornton, "Vacancy mediated substitutional diffusion in binary crystalline solids", *Prog. in Mater. Sci.* **55**, 61-105 (2010).
- [23] Q. Zhang, P.W. Voorhees, and S.H. Davis, "Mechanisms of surface alloy segregation on faceted core-shell nanowire growth", *J. Mech. Phys. Solids* **100**, 21-44 (2017).
- [24] T. Iwai, "Vacancy-mediated phase separation of binary alloy", *J. Phys. Soc. Jpn.* **68**, 3717-3728 (1999).
- [25] H. Roder, R. Schuster, H. Brune, and K. Kern, "Monolayer-confined mixing at the Ag-Pt(111) interface", *Phys. Rev. Lett.* **71**, 2086 (1993).
- [26] M.H.F. Sluiter, C. Colinet, and A. Pasturel, "Ab initio calculation of the phase stability in Au-Pd and Ag-Pt alloys", *Phys. Rev. B* **73**, 174204 (2006).
- [27] L. Vitos, A.V. Ruban, H.L. Skriver, and J. Kolla, "The surface energy of metals", *Surf. Sci.* **411**, 186-202 (1998).
- [28] J.J. Hoyt, "Molecular dynamics study of equilibrium concentration profiles and the gradient energy coefficient in Cu-Pb nanodroplets", *Phys. Rev. B* **76**, 094102 (2007).
- [29] M. Khenner, "Directed long-range transport of a nearly pure component atom clusters by the electromigration of a binary surface alloy", *Phys. Rev. Materials* **5**, 024001 (2021).
- [30] Y. Uchida and G. Lehmppfuhl, "Estimation of ad-vacancy formation energy on the Pt(111) surface by using reflection electron microscopy", *Surf. Sci.* **243**, 193 (1991).
- [31] H.M. Polatoglou, M. Methfessel, and M. Scheffier, "Vacancy-formation energies at the (111) surface and in bulk Al, Cu, Ag, and Rh", *Phys. Rev. B* **48**, 1877 (1993).
- [32] D. Wang, L. Tsau, and K.L. Wang, "Nanometer-structure writing on Si(100) surfaces using a non-contact-mode atomic force microscope", *Appl. Phys. Lett.* **65**, 1415 (1994).
- [33] The expression for ω_l is too cumbersome to be presented in a paper or in supplemental materials. It was obtained with the help of a computer algebra system Mathematica. Mathematica notebook is available on request from the author.